# Topology Optimization of Flux Switching Machine Rotors

Théodore Cherrière, S Hlioui, Mohamed Gabsi, Luc Laurent, François Louf, Hamid Ben Ahmed

# Topology Optimization of Flux Switching Machine Rotors


Théodore Cherrière
*SATIE laboratory*
*ENS Paris-Saclay, Paris-Saclay Univ., CNRS*
91190, Gif-sur-Yvette, France
theodore.cherriere@ens-paris-saclay.fr

Sami Hlioui
*SATIE laboratory*
*CY Cergy Paris Univ., Paris-Saclay Univ., CNRS*
95000, Cergy, France
sami.hlioui@ens-paris-saclay.fr

Mohamed Gabsi
*SATIE Laboratory*
*ENS Paris-Saclay, Paris-Saclay Univ., CNRS*
91190, Gif-sur-Yvette, France
mohamed.gabsi@ens-paris-saclay.fr

Luc Laurent
*LMSSC laboratory*
*CNAM, HESAM University*
75003, Paris, France
luc.laurent@lecnam.net

François Louf
*Laboratoire de Mécanique Paris-Saclay*
*Paris-Saclay Univ., ENS Paris-Saclay, CentraleSupélec, CNRS*
91190, Gif-sur-Yvette, France
francois.louf@ens-paris-saclay.fr

Hamid Ben Ahmed
*SATIE Laboratory*
*ENS Rennes*
35170, Bruz, France
benahmed@ens-rennes.fr



***Abstract*—This paper investigates the topology optimization of the rotor of a 3-phase flux switching machine with 12 permanent magnets located within the stator. The objective is to find the steel distribution within the rotor, maximizing the average torque for a given stator, permanent magnets, and electrical currents. The optimization algorithm relies on a density method based on gradient descent. The adjoint variable method is used to compute the sensitivities efficiently. Since the rotor topology depends on the current feedings, this approach is tested on several electrical periods. The obtained structures are then analyzed and classified. ERRATUM: the results below were obtained by mistake with no current in A-, B-, and C+ (*cf* the note at the end of the article).**



***Index Terms*—Density Methods, Flux-Switching Machine, Nonlinear Magnetostatics, Topology Optimization**


## I. Introduction

Topology optimization is a non-parametric conception tool that has gained significant interest from engineers. It was first developed in mechanical engineering by [1] and was introduced in electrical engineering by [2]. Several techniques have appeared, such as the level-set method [3], or the phase-field approach [4]; see [5] for an overview. Among these various methods, density-based approaches are the most popular. The geometry to be optimized is represented by a discrete density field as a pixelation on $N_e$ elements, as shown in Fig. 1.

The following optimization problem is solved:

$$\begin{aligned} &\text{find} && \boldsymbol{\rho}_{\text{opt}} = \arg\min f(\boldsymbol{\rho}) \\ &\text{subject to} && \boldsymbol{\rho} \in [0,1]^{N_e}, \end{aligned} \tag{1}$$

where $f$ is the objective function to minimize, and $\boldsymbol{\rho}$ is the vector of optimization variables, which represent the density of each mesh element. A density value of 0 represents air, and a density value of 1 represents iron in the corresponding mesh.

In order to avoid solving a combinatorial problem that may be intractable, the density methods introduce intermediate materials associated with density values strictly between 0 and 1. Their physical properties are continuously interpolated in order to use a fast gradient descent algorithm. However, these intermediate materials must be removed during optimization because they do not necessarily have a proper physical interpretation or may represent a microstructure that is complex to manufacture, see [6].

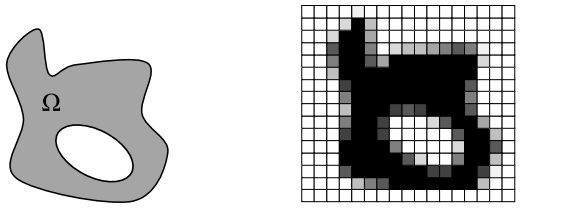


(a) Original domain Ω. (b) Density-based representation of Ω.

Fig. 1. Principle of density-based representation.

In this work, we apply a density-based topology optimization methodology to a Flux-Switching Machine (FSM). Characteristics of FSM are a passive rotor with the field inductor located in the stator only, which makes them suitable for high-speed applications. Several types of SFM exist in the literature, see [7]. The chosen test case is a 3-phase Permanent Magnet Flux Switching (PMFS) machine with 12 permanent magnets, as presented in [8] and shown in Fig. 2.

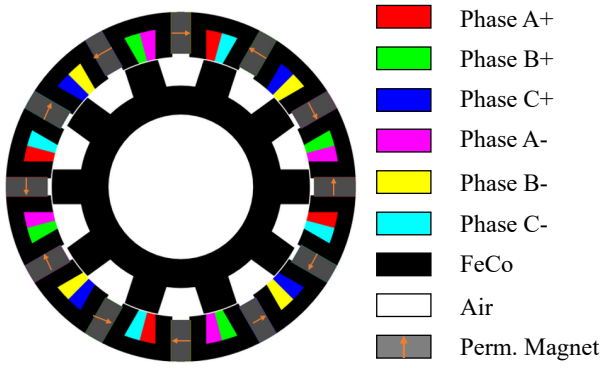


Fig. 2. Reference PMSF machine adapted from [8].

This paper is structured as follows. First, the physical equations are recalled. The optimization algorithm is then detailed. Next, the optimized designs are presented and discussed. Finally, the conclusion summarizes the essential results and draws perspectives on this work.

## II. Physical problem

### A. Material interpolation

Two possibilities are reported in the literature to interpolate the magnetic properties of intermediate materials. One can interpolate either the magnetic permeability $\mu$ as in [2] or the magnetic reluctivity $\nu = \mu^{-1}$ as in [9]. In this work, we choose to interpolate linearly the magnetic reluctivity $\nu$ of a FeCo alloy (AFK1 from Aperam):

$$\tilde{\nu}(\rho, |\mathbf{b}|) = \nu_0 + \rho \cdot (\nu_{\text{FeCo}}(|\mathbf{b}|) - \nu_0). \tag{2}$$

The corresponding BH curves are plotted in Fig. 3.

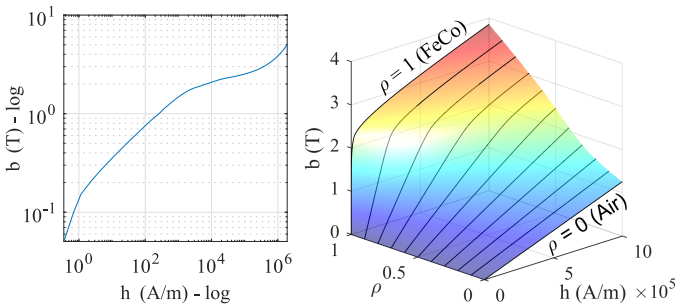


(a) Anhysteretic BH curve of FeCo.

(b) BH curves of intermediate materials obtained by (2) from air and FeCo behaviors.

Fig. 3. Magnetic behavior law used for the computation.

### B. Physical equations

From the static Maxwell's equations, one can write the magnetostatics equation for a 2D problem:

$$-\nabla.(\tilde{\nu}(\boldsymbol{\rho}, |\boldsymbol{b}|)\nabla a_z) = j_z + \nu_0 \nabla. \left( \begin{bmatrix} 0 & 1 \\ -1 & 0 \end{bmatrix} \boldsymbol{b}_r \right), \tag{3}$$

with $\tilde{\nu}$ the non-constant magnetic reluctivity of any material (intermediate or not), $j_z$ the current density, $\boldsymbol{b}_r$ the remanent flux density of permanent magnets and $a_z$ the $z$-component of the magnetic vector potential $\boldsymbol{a}$, related to the flux density by the formula $\mathbf{b} = \nabla \times \boldsymbol{a}$. (3) should be discretized to be solved numerically using, for instance, the Finite Element Method (FEM). After discretization, it reads:

$$\mathbf{K}(\boldsymbol{\rho}, \mathbf{a})\mathbf{a} = \boldsymbol{s}, \tag{4}$$

where $\mathbf{K}$ is the finite element matrix, $\mathbf{a}$ the vector containing the discretized degrees of freedom $a_z$, and $\boldsymbol{s}$ the right-hand side related to source terms. This nonlinear system is solved with the Newton-Raphson scheme:

$$\mathbf{a}_{n+1} = -\left( \frac{\mathrm{d}\boldsymbol{r}_n}{\mathrm{d}\mathbf{a}} \right)^{-1} \boldsymbol{r}_n + \mathbf{a}_n, \tag{5}$$

with $\boldsymbol{r}_n = \mathbf{K}(\boldsymbol{\rho}, \mathbf{a}_n)\mathbf{a}_n - \boldsymbol{s}$ is the residual of (4) at iteration $n$. After convergence, the torque can be computed from the flux density field within the airgap $e$ by Arkkio's method [10]:

$$T(\boldsymbol{b}) = \frac{L}{\mu_0(R_s - R_r)} \iint_e r b_r b_\theta \, \mathrm{d}s, \tag{6}$$

where $L$ is the axial length of the machine, $R_s$ and $R_r$ are the radius of the stator and the rotor, respectively.

## III. Optimization Algorithm

The purpose of the optimization is to solve the problem (1). The objective function to minimize is the opposite of the average torque (*i.e.*, the average torque should be maximized) computed with (6) on 360 angular positions along one mechanical turn. Density-based approaches use the gradient descent method. The gradient computation is non-trivial as the objective function rarely depends on $\boldsymbol{\rho}$ explicitly. Indeed, it rather depends on the physical state of the system (the magnetic field, for example), which depends implicitly on the density vector $\boldsymbol{\rho}$ through a material interpolation, such as (2), and a physical equation, such as (4). The optimization flowchart is given in Fig. 4.

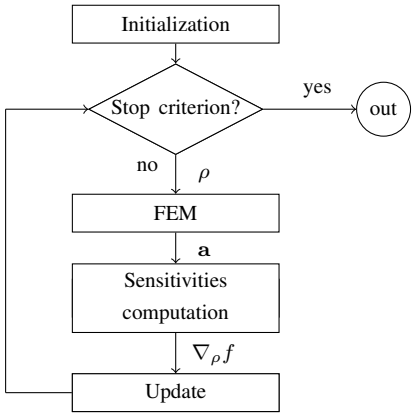


Fig. 4. Flowchart of the optimization algorithm.

### A. Sensitivities computation

The Adjoint Variable Method (AVM) is the most efficient approach to compute first-order derivatives from many variables. Once the FEM system (3) is solved, the sensitivities are computed using the adjoint state $\boldsymbol{\lambda}$, which is the solution of the following linear system:

$$\left( \frac{\mathrm{d}\boldsymbol{r}}{\mathrm{d}\mathbf{a}} \right)^T \boldsymbol{\lambda} = \frac{\partial f}{\partial \mathbf{a}}, \tag{7}$$

then the sensitivities with respect to each design variable $\rho_i$ can be calculated with:

$$\frac{\mathrm{d}f}{\mathrm{d}\rho_i} = -\boldsymbol{\lambda}^T \frac{\partial \mathbf{K}}{\partial \mathbf{a}} \mathbf{a}. \tag{8}$$

Note that (7) is linear and should be solved only once per iteration. Consequently, the average single-thread computing time per optimization iteration of AVM (34 s) is almost negligible compared to the one of the nonlinear FEM (478 s).

### B. Update

In order to accelerate the optimization and promote the real materials, the descent direction $\boldsymbol{d}$ is normalized as follows:

$$\boldsymbol{d} = -\text{sign}\left(\nabla_{\boldsymbol{\rho}} f\right), \tag{9}$$

with $\nabla_{\boldsymbol{\rho}} f$ the sensitivity vector of $f$ to the density vector $\boldsymbol{\rho}$. A simplified trust-region algorithm [11] adapts the step size heuristically according to a quality indicator:

$$q = \frac{\Delta f}{\nabla_{\boldsymbol{\rho}} f^T \cdot \Delta \boldsymbol{\rho}}, \tag{10}$$

where $\Delta f$ is the variation of the objective function, and $\Delta \boldsymbol{\rho}$ the variation of the density vector. If $q$ is too low, the iteration is rejected, and the step size is reduced. If $q$ is big enough, the iteration is accepted, and the step size can also be increased. The flowchart Fig. 5 gives more details about this algorithm.

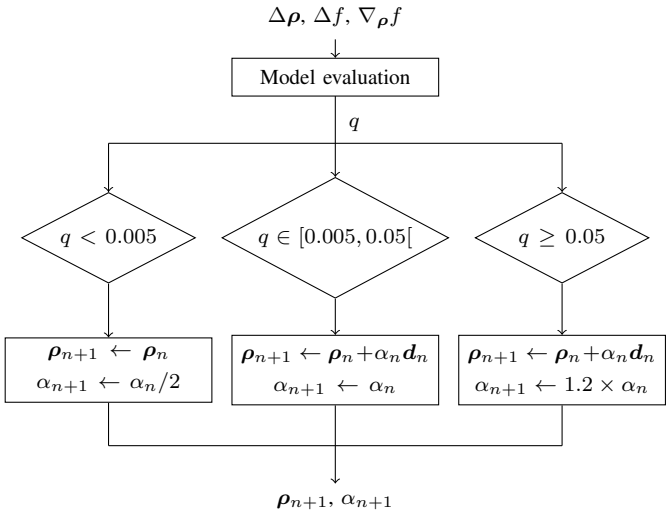


Fig. 5. Flowchart of the update algorithm.

## IV. Results and Discussion

The machine given in Fig. 2 was discretized on a mesh with 16 239 nodes and 30 666 first-order triangles. The rotor contains 11 724 triangles, each associated with a design variable. The algorithm stops after 100 iterations. The convergences of all optimizations are considered to be reached because the relative increase of the objective function is then less than 0.1 %. The FEM and MVA were implemented in Matlab 2020b and verified by comparison with the results given by GetDp [12] and centered finite differences, respectively. The current density inside a conductor $\gamma$ reads:

$$J_\gamma = J \cos\left(N\theta_m - \frac{\gamma\pi}{3}\right), \quad \gamma \in [\![1, 6]\!], \tag{11}$$

where $J = 10\,\text{A/mm}^2$ is the current density amplitude, $N$ is the number of electrical periods during one complete mechanical rotation, $\theta_m$ is the mechanical angle. The initial situation of the optimization process is given in Fig. 6. The $N$ values between 1 and 23 corresponding to different electrical frequencies were tested.

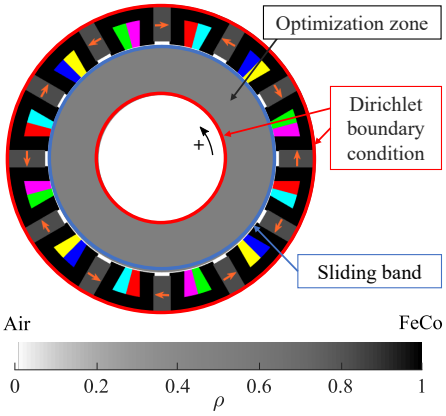


Fig. 6. Initial material distribution ($\rho = 0.5$ in the optimization zone) with boundary conditions and rotation direction.

The eight designs with the highest average torques are given in Fig. 8, and their flux densities are plotted in Fig. 9. $N = 10$ returns the highest torque at $1166\,\text{Nm/m}$. This is not a surprise since it corresponds to the configuration of the reference machine in Fig. 2 that has a $1159\,\text{Nm/m}$ torque. We also note that the number of rotor teeth $N_r$ of all the performing designs found by the algorithm is even. Indeed, the condition to have a non-zero average torque [8] reads:

$$\theta_r = \frac{\theta_s}{1 + \frac{n}{2q}}, \quad n \in \mathbb{Z}, \tag{12}$$

with $\theta_r$ the angle of a rotor cell, $\theta_s$ the angle of a stator cell, q the number of electrical phases. In the present case, $q = 3$, and there are 12 stator cells. As the number of rotor teeth $N_r = 2\pi/\theta_r$ reads:

$$N_r = 12 + 2n = 2n', \quad n' = 6 + n, \tag{13}$$

which proves the parity of suitable $N_r$. Furthermore, the final average torques given in Fig. 7 shows clearly that the algorithm failed to find performing designs for some electrical frequencies, especially for odd $N$. An example of such a "bad" structure for an odd $N$ is given in Fig. 10.

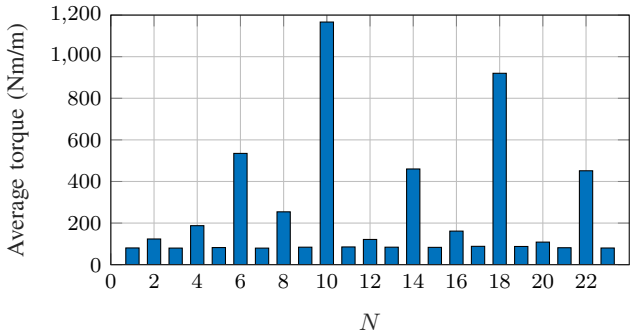


Fig. 7. Final average torques of the optimized designs.

By definition of an electrical period that corresponds to a magnetic (and necessarily mechanical) invariance, $N_r$ and $N$ are related by:

$$N_r = kN, \quad k \in \mathbb{N}^*. \tag{14}$$

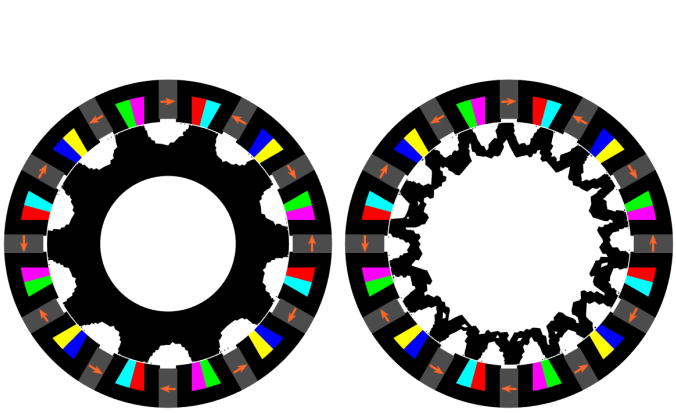

(a) $N = 10$, $\langle T \rangle = 1166\,\mathrm{Nm}$ (b) $N = 18$, $\langle T \rangle = 920\,\mathrm{Nm}$

(c) $N = 6$, $\langle T \rangle = 535\,\mathrm{Nm}$ (d) $N = 14$, $\langle T \rangle = 460\,\mathrm{Nm}$

(e) $N = 22$, $\langle T \rangle = 451\,\mathrm{Nm}$ (f) $N = 8$, $\langle T \rangle = 254\,\mathrm{Nm}$

(g) $N = 4$, $\langle T \rangle = 188\,\mathrm{Nm}$ (h) $N = 16$, $\langle T \rangle = 161\,\mathrm{Nm}$

Fig. 8. Final designs of the 8 highest torque structures in decreasing order. The color legend for the stator is given in Fig. 2, and the colorscale for intermediate materials is given in Fig. 6.

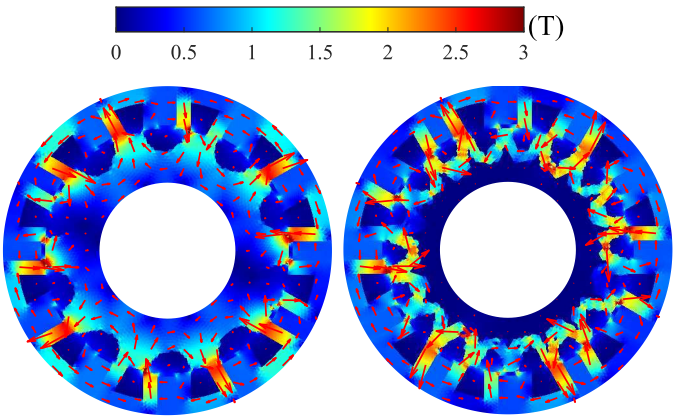


(a) $N = 10$ (b) $N = 18$

(c) $N = 6$ (d) $N = 14$

(e) $N = 22$ (f) $N = 8$

(g) $N = 4$ (h) $N = 16$

Fig. 9. Flux densities associated with the designs of Fig. 8, corresponding to $\theta_m = 0°$ with a current density $J = 10\,\mathrm{A/mm^2}$.

According to (14), the parity of $N$ does not follow from the established parity of $N_r$. However, the results found by the algorithm seem to indicate that there is no suitable rotor for odd $N$ with this type of stator.

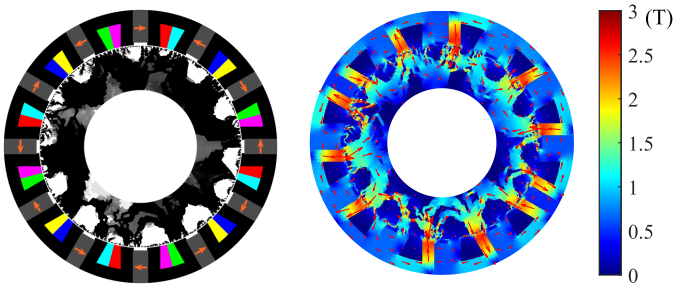


(a) Final design. (b) Associated flux density.

Fig. 10. Example of a "bad" design obtained for $N = 13$.

Note that this methodology returns traditional connected rotors with $k = 1$ such as for $N \in \{10, 14, 18\}$. The algorithm is also able to find unconventional topologies: some rotors are made from separate parts, others have $k = 2$, or both. The results for even $N$ are classified in Table I according to their $k$ value and their connectivity (*i.e.*, if the rotor is made of one part or not). We notice that some designs are uncertain and may be mixtures between the other categories represented in the other columns of Table I, such as for $N = 22$ shown in Fig. 8e or $N = 16$ shown in Fig. 8h. High $N_r$ values associated with high $N$ values may also suffer from the fixed mesh resolution that can be too coarse. Note also that some gray material may remain especially for low-torque design, for instance in Fig. 8h or Fig. 10a, because no penalization scheme was set on intermediate materials.

TABLE I
CLASSIFICATION OF THE OBTAINED ROTORS FOR EVEN $N$

| $k = 1$ | | $k = 2$ | | Uncertain |
|---|---|---|---|---|
| Connected | Disconnected | Connected | Disconnected | |
| $N = 10$ | | | $N = 2$ | $N = 12$ |
| $N = 14$ | $N = 6$ | - | $N = 4$ | $N = 16$ |
| $N = 18$ | | | $N = 8$ | $N = 20$ |
| | | | | $N = 22$ |

## V. CONCLUSION AND PERSPECTIVES

In this work, we presented and detailed a topology optimization algorithm to find a rotor that maximizes the average torque of a 3-phase PMFS machine. Several electrical frequencies were tested, and the obtained structures were analyzed and classified. These results demonstrate the method's adaptability, which has found diverse topologies from scratch. However, the algorithm found no meaningful structure for odd $N$, indicating that this electrical feeding choice may be unsuitable for producing torque, regardless of the rotor.

Further investigation is required to justify the parity of $N$ and to ensure that the provided results are not local optima, for instance with a multistart approach. More functionalities can also be added to demonstrate the usefulness of topology optimization in the design and analysis of electrical machines, including sensitivity analysis on the source terms, and the consideration of additional physics such as thermics or mechanics.

**ERRATUM**: the presented results were obtained unintentionally with no current inside the conductors A-, B-, and C+. With a proper 3-phase feeding, we find that significantly fewer $N$ values give suitable rotors. The results obtained with $N \in \{4, 10, 16\}$ are almost unchanged, but the rotors obtained with other $N$ values produce almost no torque, and their designs are similar to Figure 10a. Our conclusion regarding the adaptability of topology optimization is reinforced since suitable solutions are found even under highly unusual conditions. However, the previously obtained designs for $N \notin \{4, 10, 16\}$ should not be considered for practical applications.

## REFERENCES


[1] M. P. Bendsøe, "Optimal shape design as a material distribution problem," *Structural Optimization*, vol. 1, no. 4, pp. 193–202, 1989.

[2] D. N. Dyck and D. A. Lowther, "Automated design of magnetic devices by optimizing material distribution," *IEEE Transactions on Magnetics*, vol. 32, no. 3 PART 2, pp. 1188–1192, 1996.

[3] Y. S. Kim and I. H. Park, "Topology Optimization of Rotor in Synchronous Reluctance Motor Using Level Set Method and Shape Design Sensitivity," *IEEE Transactions on Applied Superconductivity*, vol. 20, no. 3, pp. 129–133, 2010.

[4] J. S. Choi, K. Izui, S. Nishiwaki, A. Kawamoto, and T. Nomura, "Topology optimization of the stator for minimizing cogging torque of IPM motors," *IEEE Transactions on Magnetics*, vol. 47, no. 10, pp. 3024–3027, 2011.

[5] F. Campelo, J. A. Ramírez, and H. Igarashi, "A survey of topology optimization in electromagnetics : considerations and current trends," pp. 2–47, 2010. [Online]. Available: https://www.academia.edu/2751679/A_survey_of_topology_optimization_in_electromagnetics_considerations_and_current_trends

[6] M. P. Bendsøe and O. Sigmund, "Material interpolation schemes in topology optimization," *Archive of Applied Mechanics*, vol. 69, no. 9-10, pp. 635–654, 1999.

[7] J. T. Shi, Z. Q. Zhu, D. Wu, and X. Liu, "Comparative study of synchronous machines having permanent magnets in stator," *Electric Power Systems Research*, vol. 133, pp. 304–312, 2016.

[8] E. Hoang, H. Ben Ahmed, and J. Lucidarme, "Switching flux permanent magnet polyphased synchronous machines," in *EPE 97*, Trondheim, 1997, pp. 3903–3908.

[9] J. S. Choi and J. Yoo, "Structural optimization of ferromagnetic materials based on the magnetic reluctivity for magnetic field problems," *Computer Methods in Applied Mechanics and Engineering*, vol. 197, no. 49-50, pp. 4193–4206, 2008.

[10] A. Arkkio, "Analysis of Induction Motors Based on the Numerical Solution of the Magnetic Field and Circuit Equations." Ph.D. dissertation, Helsinki University of Technology, 1987.

[11] J. Nocedal and S. J. Wright, *Numerical optimization*, P. Glynn and S. M. Robinson, Eds. Springer, 2006.

[12] P. Dular, C. Geuzaine, F. Henrotte, and W. Legros, "A general environment for the treatment of discrete problems and its application to the finite element method," *IEEE Transactions on Magnetics*, vol. 34, no. 5, pp. 3395–3398, Sep. 1998.